Cenozoic Exhumation History of the Eastern Margin of the Northern Canadian Cordillera

Ryan Mckay, Eva Enkelmann, Thomas Hadlari, William Matthews, Frédéric Mouthereau

Tectonics

Key Points:

- Apatite (U-Th-Sm)/He data record late Eocene-early Oligocene and younger exhumation in the Richardson Mountains
- Observed age dispersion may correspond to variations in sediment sources and predeposition cooling histories
- Deformation along the eastern margin of the Northern Cordillera may have been driven by changes of the North American Plate motion

Correspondence to:

E. Enkelmann,
eva.enkelmann@ucalgary.ca

Cenozoic Exhumation History of the Eastern Margin of the Northern Canadian Cordillera

Ryan McKay[1], Eva Enkelmann[1], Thomas Hadlari[2], William Matthews[1], and Frédéric Mouthereau[3]

[1]Department of Geoscience, University of Calgary, Calgary, AB, Canada, [2]Natural Resources Canada, Calgary, AB, Canada, [3]Géosciences Environnement Toulouse, Université de Toulouse, UPS, Université Paul Sabatier, CNRS, IRD, Toulouse, France

Abstract New low-temperature thermochronology data from clastic sedimentary rocks in the northern Richardson Mountains, Canada, indicate significant exhumational cooling during late Eocene–early Oligocene time. Apatite (U-Th-Sm)/He (AHe) data were collected from 19 Proterozoic–Paleocene rocks across a 115 km transect. Eighty-eight single-grain AHe dates range from 16–300 Ma and are generally younger than stratigraphic ages, indicative of thermal resetting by burial. Additionally, zircon (U-Th)/He (ZHe) dates from two Proterozoic–Cambrian rocks range from 49–123 Ma and suggest burial to >160°C. In contrast, ZHe dates from Jurassic sandstones are older than the stratigraphic age, which limits maximum burial to <160°C. Thermal history modeling reveals three phases of cooling, during the Paleocene–early Eocene (>65–50 Ma), late Eocene–early Oligocene (40–30 Ma), and late Oligocene–early Miocene (30–15 Ma). Most samples cooled during the first and second phases, whereas the third phase is less well constrained. In general, most rocks were below the sensitivity of AHe analysis since the early–middle Miocene. The results suggest a previously unrecognized phase of inferred deformation in the northern Richardson Mountains between 40–30 Ma. Our findings contribute to previous work that recognizes Late Cenozoic deformation along the eastern margin of the Northern Cordillera. We further investigated the potential mechanisms of this widespread deformation and suggest exhumation may relate to kinematic changes of the North American plate relative to structural trends along the margin of the Northern Cordillera.

Plain Language Summary We are interested in learning when and why the Richardson Mountains formed. To do this, we use a method called thermochronology, which analyzes isotopes of a mineral to determine its temperature history. During mountain building, rocks that were buried at depth are brought closer to the surface due to deformation, uplift, and erosion. Thermochronology can tell us how far in the past this process occurred. We measured 19 rock samples and used a computer program to model thermal histories based on the thermochronology dates. We found three stages of accelerated cooling in the thermal history. The oldest stage was already known: the rocks were buried until about 65 million years ago (Ma), and then started to cool due to mountain-building processes. The next younger stage of cooling occurred between 40 and 30 Ma. The youngest stage shows that some cooling occurred as late as 15 Ma. We found that the timing of deformation is similar to nearby mountain belts, which supports a widespread driving mechanism for deformation that affected a large area. We suggest that this driving mechanism could be the motion of the North American craton and its changes in pace and direction over time.

1. Introduction

The Richardson Mountains are a Late Cretaceous–Cenozoic fold-and-thrust belt located north of the Mackenzie Mountains, which together form the eastern margin of the Northern Canadian Cordillera (Figure 1). Unlike their southern counterpart, the Canadian Rocky Mountains, these mountain ranges are tectonically active today, attracting geophysical and geological investigations that aim to quantify Cenozoic to recent deformation (e.g., Enkelmann et al., 2019; Hyndman, Cassidy, et al., 2005; Hyndman, Flück, et al., 2005; Lane, 1998; Leonard et al., 2008; Mazzotti & Hyndman, 2002; Powell et al., 2019). The main unresolved questions are: what is the spatial and temporal pattern of Cenozoic to modern deformation, and what are the driving forces?
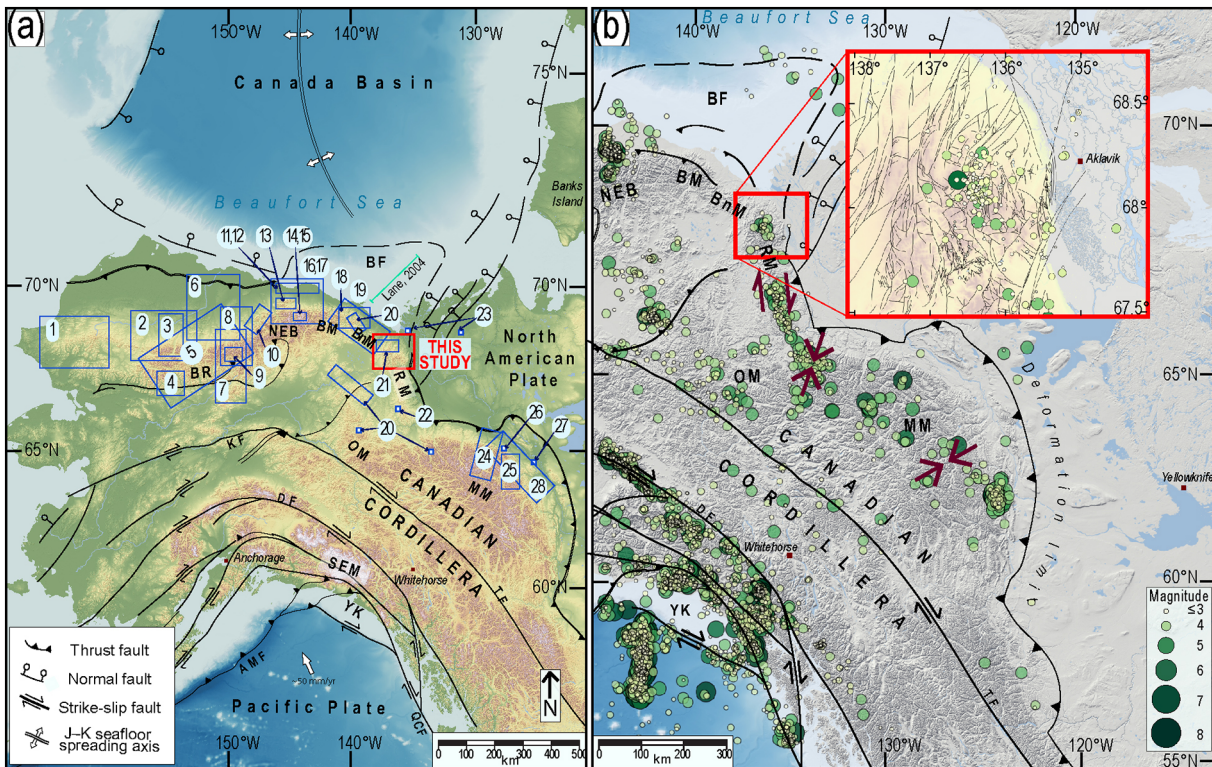
Figure 1. (a) Topographic map of northwestern North America with main geographic and tectonics features. Regions of previous thermal-history studies are shown as white boxes. References: (1) Ceraddock et al. (2018); (2) Moore et al. (2004); (3) Cole et al. (1997); (4) Blythe et al. (1997); (5) Murphy et al. (1994); (6) O'Sullivan (1996); (7) Blythe et al. (1996); (8) O'Sullivan et al. (1997); (9) O'Sullivan, Moore, et al. (1998); (10) O'Sullivan, Wallace, et al. (1998); (11) Parris et al. (2003); (12) Potter et al. (2004); (13) O'Sullivan and Wallace (2002); (14) O'Sullivan et al, (1995); (15) Peapples et al. (1997); (16) O'Sullivan and Decker (1990); (17) O'Sullivan et al. (1993); (18) Bigot-Buschendorf et al. (2019); (19) Bigot-Buschendorf (2015); (20) Lane and Issler (2011); (21) O'Sullivan and Lane (1997); (22) Issler and Lane (2016); (23) Issler et al. (2012); (24) Enkelmann et al. (2019); (25) Powell et al. (2016); (26) Powell et al. (2018); (27) Issler et al. (2005); (28) Powell et al. (2019). (b) Seismicity and current tectonics of the Canadian Cordillera and eastern Alaska showing earthquakes of magnitudes ≥3 (USGS–ANSS Catalogue, 1985–2019). Red arrows show general deformation regimes along the eastern margin of the Cordillera after Hyndman, Flück, et al. (2005). Inset topographic map shows seismicity of the northern Richardson Mountains. BF, Beaufort Foldbelt; BM, British Mountains; BnM, Barn Mountains; BR, Brooks Range; DF, Denali Fault; KF, Kaltag Fault; MM, Mackenzie Mountains; NEB, Northeastern Brooks Range; NEB, Northeastern Brooks Range; OM, Ogilvie Mountains; PSMF, Phillip Smith Mountain Front; QCF, Queen Charlotte Fault; RM, Richardson Mountains; SEM, Saint Elias Mountains; TF, Tintina Fault; YK, Yakutat Microplate.

The main purpose of this study is to quantify timing and amount of exhumation in the northern Richardson Mountains using low-temperature thermochronological methods. We present new apatite and zircon (U-Th-Sm)/He (AHe, ZHe) data from 19 samples collected from the northern Richardson Mountains that reveal the timing and magnitude of rock exhumation during the Cenozoic. Our data set expands the spatial range from previous studies and uses methods sensitive to both higher and lower temperatures than previously investigated. We use thermal history modeling to determine the possible time-temperature (*t-T*) histories that are supported by our data. We also conducted numerical modeling to investigate the potential influence of individual grain parameters, such as the predepositional thermal histories of the grains. Our results provide clear evidence of Paleocene–early Eocene and late Eocene–early Oligocene cooling phases and a less prominent late Oligocene–early Miocene cooling phase. We compare our results from the northern Richardson Mountains with those reported from the Cordilleran margin to the west (Brooks Range) and the south (Mackenzie Mountains). We investigate the possibility of the North American plate motion as a possible driver for deformation by comparing the temporal changes of plate motion velocities and obliquity to the existing structural trends with phases of cooling along the eastern margin of the Northern Cordillera.
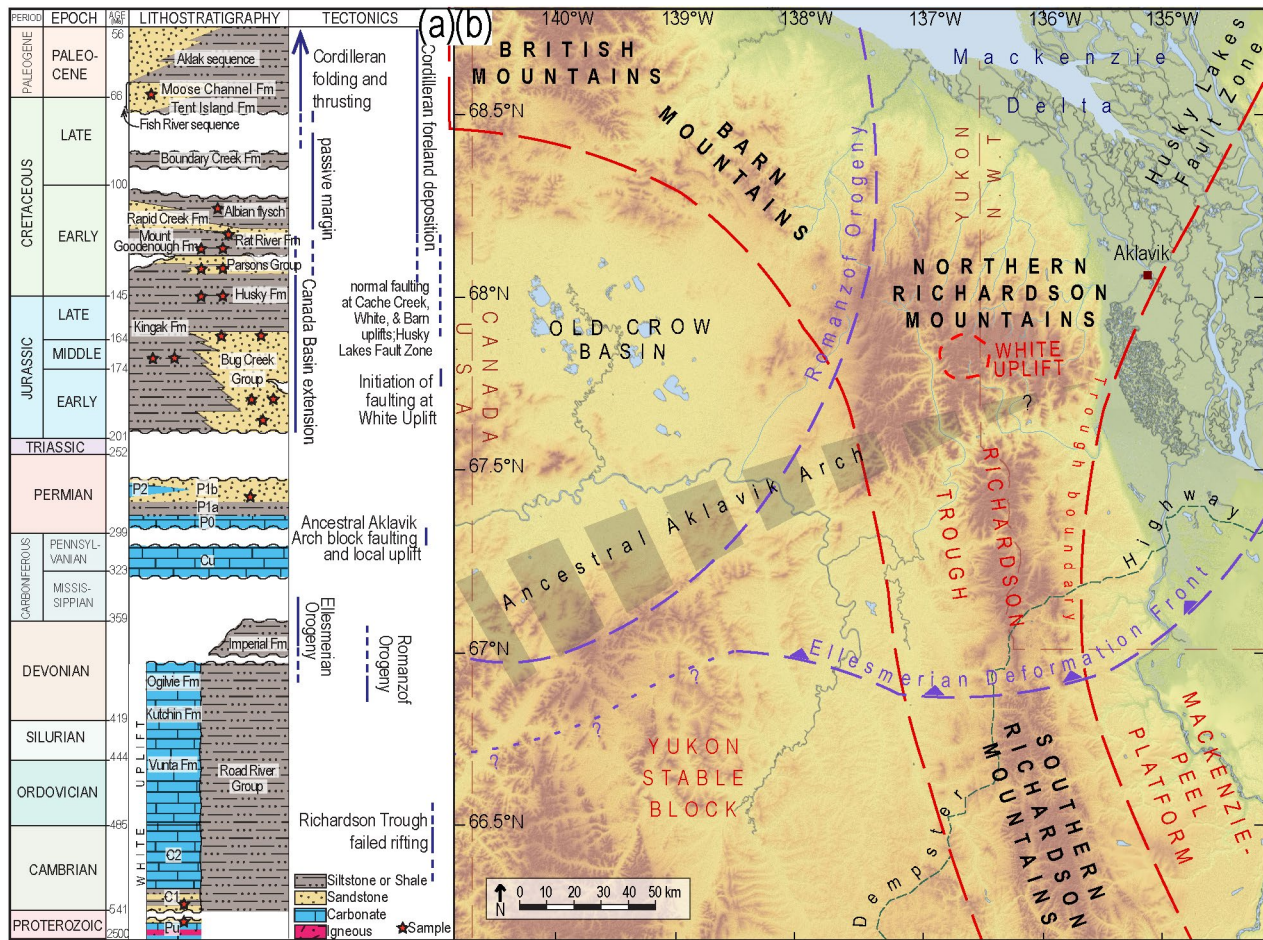
Figure 2. (a) Stratigraphic column of the northern Richardson Mountains showing generalized tectonic phases and local faulting events. Stratigraphy compiled from Dixon (1996b) and Dyke (1996). Red stars indicate approximate stratigraphic positions of samples. (b) Map of the Richardson Mountains and surrounding area showing paleogeographic features. Dashed red lines delimit the lower Paleozoic Richardson Trough and carbonate platforms. Dashed purple lines show limits of known deformation from the Devonian Romanzof Orogeny and Devonian–Carboniferous Ellesmerian Orogeny, from Lane (2007). The dark gray shaded area shows the location of latest Carboniferous–early Permian Ancestral Aklavik Arch of Jeletzky (1963).

2. Background

The northern Richardson Mountains resulted from thin-skinned deformation of Proterozoic–Paleocene clastic rocks against the west-dipping cratonic margin of ancestral North America (Lane, 1996, 1998). The dominantly NNE structural grain roughly parallels the underlying cratonic margin and was additionally inherited from a complex geological and structural history that preceded Cordilleran contraction (Figure 2; Cook et al., 1987; Lane, 1998; Lane & Dietrich, 1995; Norris, 1996). Pre-Cambrian and lower Paleozoic rocks are only exposed along the western flank of a tilted fault block known as White Uplift (Figures 2 and 3; Dyke, 1996). White Uplift originated as an isolated Cambrian–Devonian carbonate platform that developed within the Richardson Trough, a northward-broadening failed rift graben flanked by shallow-water carbonates (Figure 2; Morrow, 1999; Rohr et al., 2011).

Two major phases of orogenesis affected the Canadian Arctic margin during the mid-Paleozoic (Lane, 2007). These are the late Early Devonian to earliest Middle Devonian Romanzof Orogeny and the latest Devonian to Early Carboniferous Ellesmerian Orogeny (Figure 2; Dyke, 1996; Lane, 2007; Lane & Mortensen, 2019). The Jurassic and Early Cretaceous were characterized by extension and rifting that culminated in the opening of the Canada Basin (Figure 1). Regional extension and thinning of continental lithosphere occurred as early as 195 Ma (Grantz et al., 2011; Pease et al., 2014) with rifting and sea floor spreading during the Early Cretaceous (134–117 Ma; Grantz et al., 2011; Helwig et al., 2011). In the Richardson Mountains, Jurassic
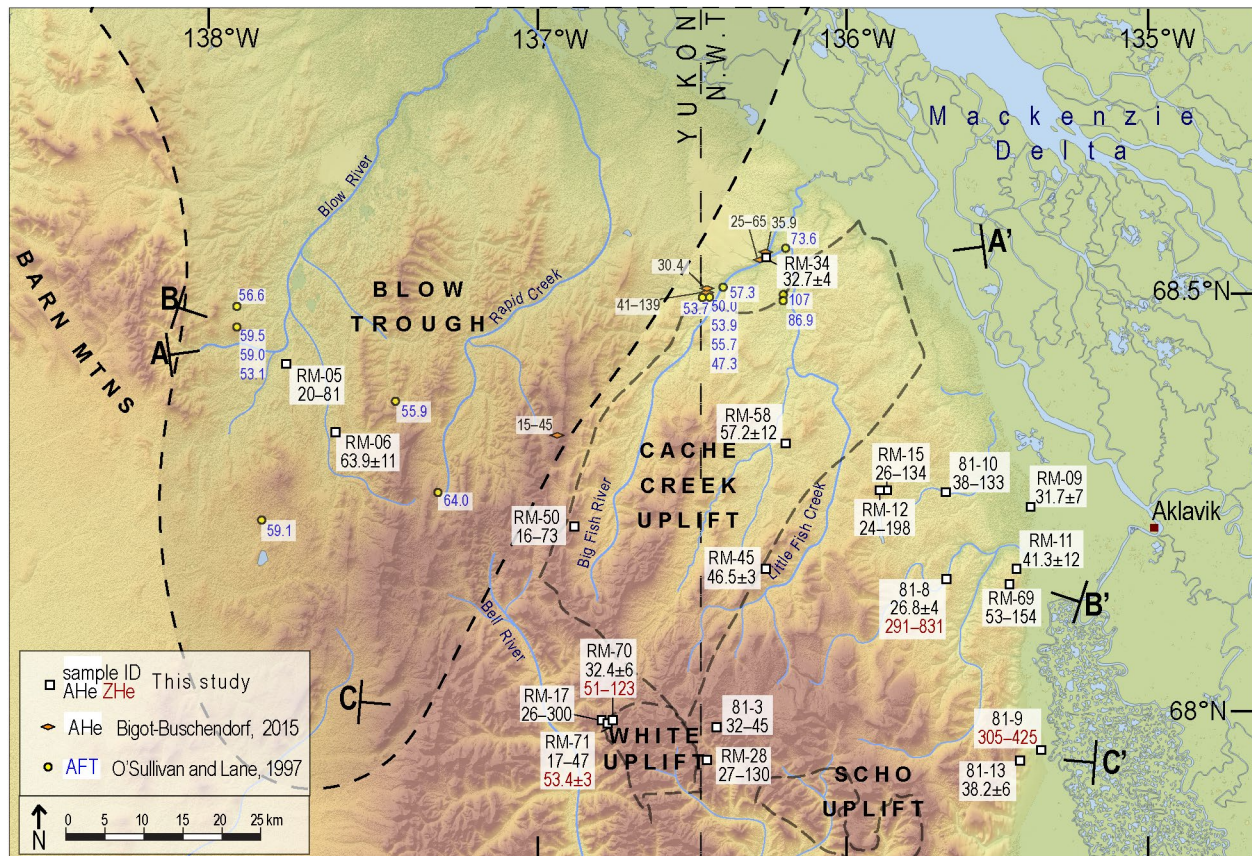
Figure 3. Topographic map of the northern Richardson Mountains showing new and published apatite and zircon (U-Th-Sm)/He data (AHe and ZHe; mean ages and standard deviation, or age range) and apatite fission track ages (AFT). The locations of paleogeographic features are outlined in black dashed line. The profile lines (A–A′, B–B′, and C–C′) show the extent of swath profiles in Figure S9.

and Lower Cretaceous rocks formed by epicontinental sedimentation (Dixon, 2004; Young, 1973) and generally represent nearshore and shelf facies deposits. Rift-associated Late Jurassic–Early Cretaceous extension resulted in regional unconformities and normal faulting (Dixon, 1992, 1993). Blow Trough developed as a graben and was flanked by Barn Uplift to the west and by Cache Creek Uplift and White Uplift to the east (Figure 3; Dixon, 1996a, 2004; Poulton, 1996; Poulton et al., 1982).

During the latest Early Cretaceous (~113–100 Ma), the primary sediment source regions shifted to west and southwest (Dixon, 1996a, 2004). This change in provenance from earlier cratonic and Devonian clastic wedge rocks is due to the encroachment of the Cordilleran thrust front to the central Brooks Range and to the southwestern Mackenzie Mountains (Blythe et al., 1996; Powell et al., 2016). Over 4 km of Albian flysch strata are preserved in Blow Trough, representing distal Cordilleran foreland deposits (Blythe et al., 1996; Dixon, 1996b; Young, 1977). A regional unconformity divides the Albian succession from overlying Late Cretaceous and Paleocene deposits (Figure 2a; Dixon, 1993). Regional east- and northeast-directed Cordilleran contraction initiated in the latest Cretaceous. Deformed strata onshore constrain the timing of contraction to Paleocene and younger. Additionally, offshore seismic reflection data record deformation of the Beaufort Foldbelt during the early, middle, and late Eocene, late Oligocene and late Miocene (Dixon et al., 1992; Lane & Dietrich, 1995). Onshore age controls for late Cenozoic deformation are limited, and there is no clear record of deformation since the early Eocene. Today, earthquakes of magnitudes up to 6.6 have been recorded in the Richardson Mountains (Figure 1b; Earthquakes Canada, 2019) and the maximum magnitude is calculated to be ~7.5 based on fault characteristics (Hyndman, Cassidy, et al., 2005; Hyndman, Flück, et al., 2005). Earthquake focal mechanisms are predominantly strike-slip in the Richardson Mountains (Hyndman, Cassidy, et al., 2005; Hyndman, Flück, et al., 2005). Thrust faults in this region show striations that indicate north–northeast-directed oblique or strike-slip displacement (Lane & Dietrich, 1995).

3. Methods

We used AHe and ZHe analyses to constrain the timing and amount of rock cooling that can be related to exhumation and erosion. The (U-Th-Sm)/He method relies on the alpha decay of radioactive isotopes of uranium (^{238}U, ^{235}U), thorium (^{232}Th), and samarium (^{147}Sm) that produced helium (e.g., Harrison & Zeitler, 2005). Helium diffuses out of the mineral at high temperatures but starts to be increasingly retained during cooling through a temperature window known as the Partial Retention Zone (PRZ). The PRZ ranges ~85°C–40°C for apatite (Flowers et al., 2009; Shuster et al., 2006; Wolf et al., 1998) and ~200°C–50°C for zircon (e.g., Guenthner et al., 2013) and differs for individual grains depending on grain size, radiation damage, and thermal history (Flowers et al., 2009; Guenthner et al., 2013). In sedimentary rocks, single-grain dates may also vary due to inheritance of helium and radiation damage from their pre-depositional (i.e., source rock) histories (e.g., Guenthner et al., 2015) or due to compositional variations (Armstrong, 2005).

We collected samples that are located primarily along a 115 km-long northwest-southeast transect through the Richardson Mountains (Figure 3). We aimed to collect coarser-grained sandstones, however, rock exposures are rare and the dominant lithologies are fine-grained clastic sedimentary rocks (see sample location on geologic map in Figure S1). We conducted apatite and zircon mineral separation on 54 rock samples using standard techniques of crushing, sieving, and magnetic and heavy liquid separation. Of these samples, only 19 yielded apatite and zircon suitable for analysis. Two to six crystals from each sample were selected using a Zeiss stereomicroscope, measured and packaged into individual Nb tubes. The selected grains are ideally euhedral, unbroken, inclusion-free, and >70 μm in width. The grain dimensions and morphology are used to calculate a geometric correction factor (F_T) that accounts for the ejection of alpha particles from the grain (Farley et al., 1996). The (U-Th-Sm)/He analyses were conducted at the Geo- and Thermochronology Lab at the University of Calgary. A full description of the measurement method can be found in the supporting information (Text S1). Helium was extracted in an Applied Spectra Alphachron helium line and quantified by external calibration to a known volume of introduced ^{3}He. Parent nuclides were determined by isotope dilution (U and Th) or external calibration (Sm) using methods modified after those of Evans et al. (2005). Final ages were calculated using a Taylor expansion of the He ingrowth equation and corrected for alpha-ejection using an in-house spreadsheet.

4. Results

We present 88 new AHe dates from 19 samples (Table S1), and 20 new ZHe dates from four samples (Table S2). The AHe dates range between 16–300 Ma and show significant intrasample dispersion. Generally, the AHe dates are younger than the stratigraphic ages of the rocks, indicative of thermal resetting by burial (Figure 4). Mean sample ages and their standard deviation were calculated for nine samples, ranging from 26.8 ± 3.6 Ma to 63.9 ± 10.8 Ma (Table S1, Figure 3). AHe dates from the remaining 10 samples (45 grains) yielded standard deviations >30% and were not used to calculate mean sample ages. Thus, in Figure 3, we show the range of AHe dates for these samples. Overall, the majority (65%) of all AHe dates range between 24 Ma and 56 Ma (Table S1, Figure S2).

Dispersion in AHe dates is commonly attributed to individual grain parameters such as grain size and radiation damage, which affect helium retention (Farley, 2000; Flowers et al., 2009). In order to investigate these dependencies, we plotted single-grain AHe dates against the equivalent spherical radius (R_s), which is the radius of a sphere with the same surface area-to-volume ratio as the measured grain (Figure S3; Wolf et al., 1996). Additionally, we plotted AHe dates against the effective uranium concentration (eU = [U] + 0.235 × [Th]), which is a proxy for radiation damage (Figure S3; Shuster et al., 2006). In general, there are no obvious correlations between R_s and the AHe dates, but some older single-grain dates can be explained by their comparatively large grain sizes (e.g., samples RM-45, RM-50, and 81-13 in Figures S3a and S3b). Similarly, there is no apparent correlation between AHe date and eU that explains the data dispersion (Figures S3c and S3d). However, in clastic sedimentary rocks, eU is likely an imperfect proxy of radiation damage because the grains have experienced variable pre-depositional thermal histories. Radiation damage accumulates in grains that have spent prolonged periods at temperatures below their annealing thresholds, in addition to grains with higher eU (Shuster & Farley, 2009). Thus, a given low-eU grain with a protracted predepositional history can accumulate significant radiation damage that impedes helium
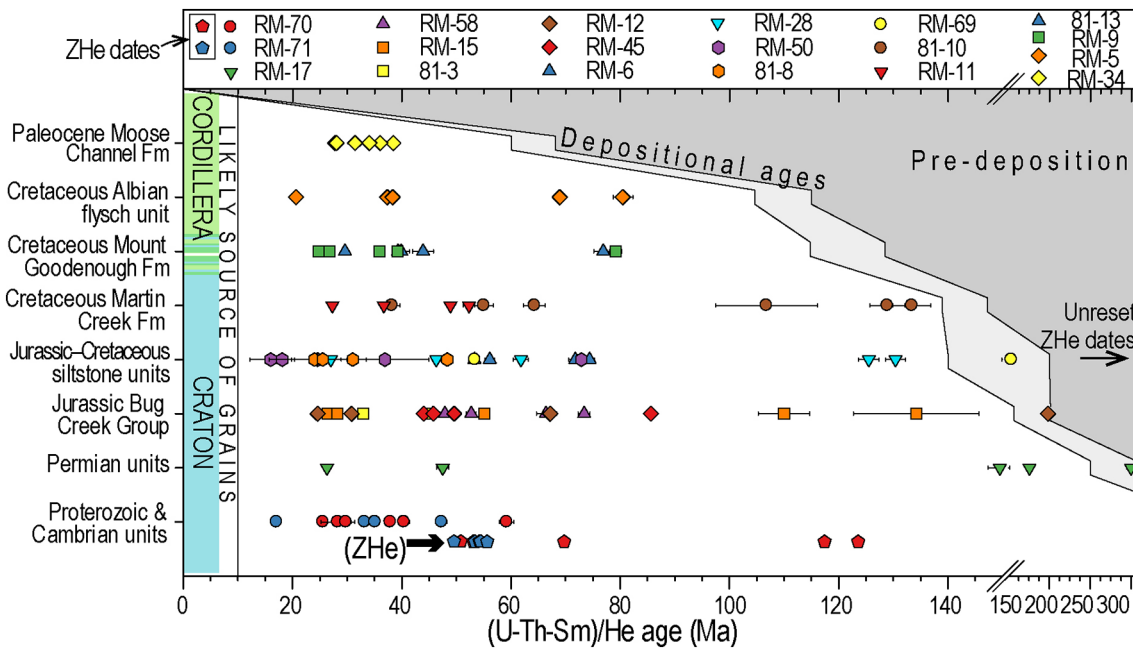
Figure 4. Apatite and zircon (U-Th-Sm)/He (AHe, ZHe) dates plotted against the stratigraphic intervals of the samples (1σ error bars). The light gray band is the depositional age and the dark gray area is the time prior to deposition. The Jurassic–Cretaceous siltstone unit includes the Husky and Kingak formations.

diffusion. We explored the influence of pre-depositional histories on the AHe dates using forward thermal history modeling. The effect of radiation damage and grain size are also considered for inverse thermal history modeling, which we used for the interpretation of our data (see below). Other potential sources of dispersion are more difficult to quantify, such as the effects of undetected inclusions, U-Th zonation, broken grains, and [4]He implantation from external phases (e.g., Farley et al., 2011; Gautheron et al., 2012). Due to the low apatite yield of our samples and the sedimentary lithologies, we dated a number of imperfect grains (i.e., broken ends, highly rounded, rough surfaces) and thus grain quality is another source of the observed data dispersion.

We also report 20 new single-grain ZHe ages from samples RM-70 and RM-71 of Proterozoic and Cambrian strata, and from samples 81-8 and 81-9 of the upper Jurassic Husky Formation (Figures 3 and 4; Table S2). The ZHe ages in the Proterozoic and Cambrian samples are younger than the stratigraphic age and indicate thermal resetting, whereas in the Jurassic samples the ZHe ages are older and not reset (Figure 4). The reset ZHe ages range 51–123 Ma for sample RM-70 and 49–56 Ma for RM-71 (mean age 53.4 ± 2.5 Ma). The unreset ZHe ages range between 291–831 Ma for sample RM 81-8, and between 305–425 Ma for 81-9.

5. Thermal History Modeling

5.1. Inverse Thermal History Modeling

We investigated the range of possible thermal histories that are consistent with the measured AHe data using the inverse mode of HeFTy (v1.9.3; Ketcham, 2005) and the radiation damage accumulation and annealing models for helium diffusion kinetics in apatite (Flowers et al., 2009) and zircon (Guenthner et al., 2013). For each sample, a Monte Carlo approach is used to generate thousands of independent time-temperature (*t-T*) paths that are then evaluated using a goodness-of-fit between the modeled and the measured single-grain data. The model output is an envelope of *t-T* paths that illustrates the range of viable thermal histories that can satisfy the measured data. Information on our modeling procedure and results are presented in the supplement information (Text S2).

The results of the inverse *t-T* path modeling are summarized in Figure 5 and individual results for each sample are shown in Figure S4 and S5. Overall, we identified three phases of cooling within our data: cooling that initiated in the Paleocene–early Eocene at >65–50 Ma (Figure 5b; Group 1); cooling in the late Eocene–
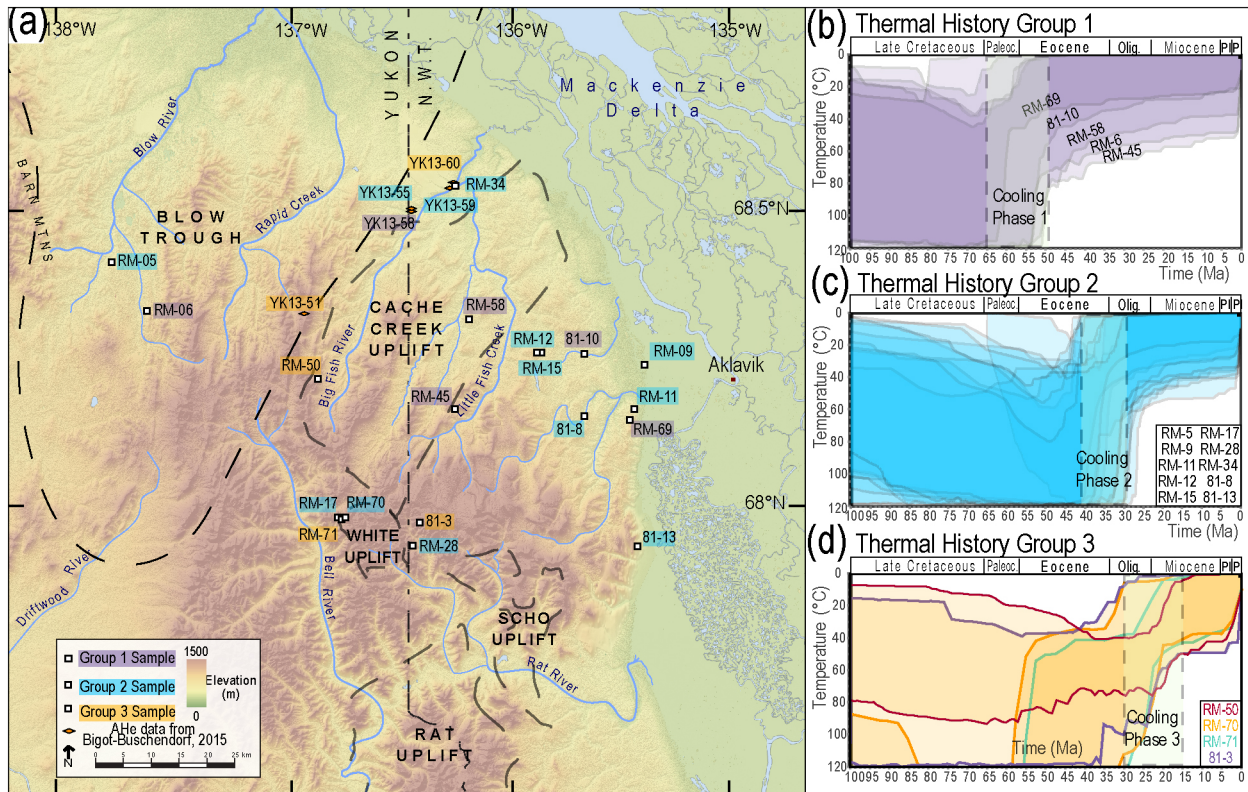
Figure 5. (a) Topographic map of the northern Richardson Mountains showing sample location from this study and from Bigot-Buschendorf (2015), with sample ID labels colored according to interpreted cooling phases. (b–d) Inverse thermal history models from HeFTy (Ketcham, 2005) compiled based on similar thermal histories. Envelopes show the range of possible time-temperature path solutions that fit the measured data. Pale rectangles indicate interpreted phases of exhumational cooling. Individual HeFTy models are presented in Figures S4 (this study) and S8 (Bigot-Buschendorf, 2015).

Oligocene between 40 and 30 Ma (Figure 5c; Group 2); and Oligocene–early Miocene cooling between 30 and 15 Ma (Figure 5d; Group 3). The amount of recorded cooling varies widely and some samples indicate multiple phases of cooling. For example, samples RM-69 and RM 81-10 indicate rapid cooling to below 40°C by 65–50 Ma, whereas samples RM-6, RM-45, and RM-58 allow for a more protracted thermal history after the initial cooling phase (Figure 5b; Group 1). Most samples show overlapping modeled t-T solutions that together suggest accelerated cooling during the late Eocene–Oligocene (Figure 5c; Group 2). The models of the four samples that record the latest cooling phase show significant variation in cooling time and rate (Figure 5d; Group 3), indicating that some individual grains record earlier cooling phases whereas others record the latest cooling. This includes the t-T histories of samples RM-71 and RM-70 that include ZHe data and clearly show two stages of cooling in the Paleocene–early Eocene and the late Oligocene (Figure 5d and Figure S4). Overall, most samples were near surface and below the sensitivity of AHe analysis by 30 Ma.

5.2. Forward Thermal History Modeling

The inverse modeling approach implicitly assumes that each of the grains share a single predepositional thermal history. However, our ZHe results and former provenance studies indicate that the sediments were derived from multiple source rocks and grains were recycled extensively (Beranek et al., 2010; Colpron et al., 2018; Hadlari et al., 2012, 2015). Helium and radiation damage are inherited from source rock thermal histories, resulting in a non-zero date at the time of deposition and increased closure temperature of the AHe system (e.g., Fox et al., 2019; Guenthner et al., 2015; Shuster et al., 2006). Accordingly, AHe date–eU relationships within a sample will not necessarily adhere to the positive trend predicted by helium diffusion models (e.g., Flowers et al., 2009), particularly if some grains were at low temperatures (below the diffusion threshold) for a prolonged period prior to deposition. To explore the influence of the predepositional thermal history of a grain on the resulting AHe dates derived from sedimentary rocks, we modeled variable
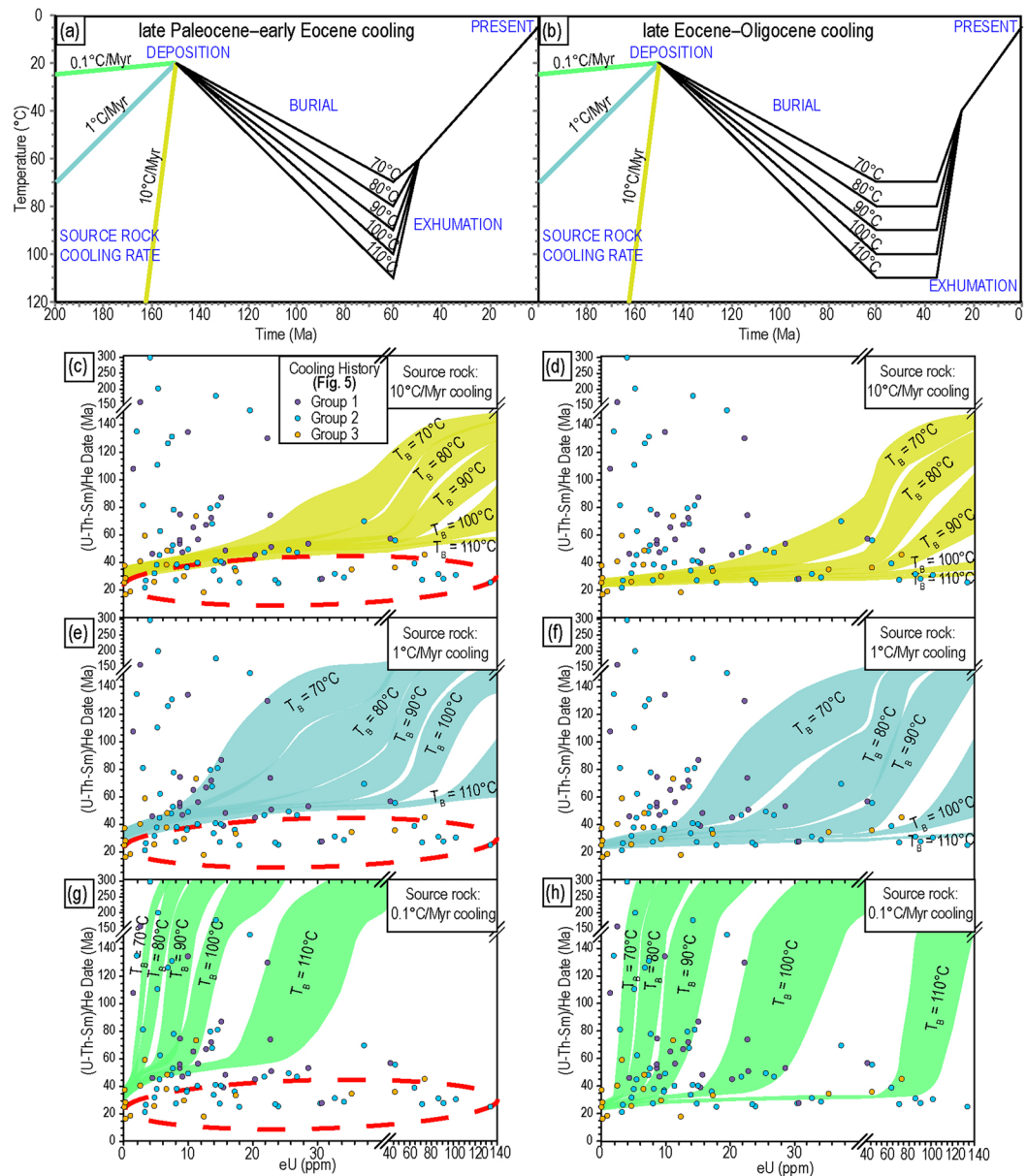
Figure 6. Results of modled apatite (U-Th-Sm)/He (AHe) date-eU envelope derived from forward thermal history modeling using HeFTy (Ketcham, 2005). Measured AHe data set shown as colored symbols. The models show the expected date-eU relationship for accelerated post-depositional cooling during (a) late Paleocene–early Eocene and (b) late Eocene–Oligocene. The models show the influence of pre-depositional (source rock) cooling rates of (c and d) 10 °C/Myr, (e and f) 1 °C/Myr, and (g and h) 0.1 °C/Myr and postdepositional burial temperatures $T_B = 70°C–110°C$ in increments of 10°C. The colored envelopes show the expected range of data for $R_s = 30–60$ µm and $r_{mr0} = 0.75$ using the tested parameters. The dashed red line denotes the measured data that are not accommodated by the modeled thermal history of panel (a).

source rock cooling rates using the forward mode of HeFTy (Ketcham, 2005). More information on our forward model procedures and results can be found in the supporting information (Text S2).

Our results indicate that for a given eU value and maximum burial temperature, a slowly cooled sediment source rock will generate older AHe dates than a rapidly cooled source rock (Figure 6). The models demonstrate that burial temperatures well above the AHe PRZ (>100°C) will not necessarily induce complete thermal resetting. We tested two *t-T* histories and found that a Late Paleocene–early Eocene cooling (Figure 6a) cannot account for the many young AHe dates in our sample set (red dashed circle in Figures 6c, 6e,

and 6g). A late Eocene–Oligocene cooling phase (Figure 6b), can reproduce the full array of AHe dates and associated eU values if variable pre-depositional grain histories are considered (Figures 6d, 6f, and 6h). The inheritance envelopes generally predict that older AHe dates correspond to lower burial temperatures (Figure 6). We estimated maximum burial temperatures for our samples by comparing the AHe date-eU data of individual samples to the inheritance envelopes generated for specific burial temperatures (Figure S7). Overall, our results from forward modeling suggest that; (1) the thermal history of the sediment source rocks is the most likely cause of AHe date dispersion in our study; (2) a major cooling phase subsequent to late Paleocene–early Eocene cooling is required to describe our data; and (3) maximum burial temperatures were approximately 70°C–90°C for most samples in our study area, with the highest temperatures of 90°C–110°C (RM-34).

6. Discussion

6.1. Stratigraphic and Spatial Patterns of Sediment Burial

Thermochronology data are sensitive to temperature changes and can be used to quantify the burial of sediment. The AHe dates of our samples from the northern Richardson Mountains are generally younger than the stratigraphic ages, which is a first-order indication of burial to above the AHe PRZ (>75°C–80°C; Figure 4). However, six of our samples exhibit highly dispersed data and have single-grain dates that predate Cordilleran orogenesis (greater than ~100 Ma). In general, AHe data from Proterozoic–Cambrian strata show less AHe date dispersion than Permian–Lower Cretaceous strata (Figure 4). The amount of dispersion decreases significantly for Upper Cretaceous strata and is the lowest for Paleocene strata. These findings suggest elevated burial temperatures during Cretaceous–Paleogene time to thermally reset the stratigraphically young samples. However, this burial phase apparently did not cause total helium diffusion in grains from the older (Permian–Lower Cretaceous) samples, or else the AHe dates would at least be as young as ~100 Ma. We generally anticipated that our AHe dates would be fully reset by this Cretaceous–Paleogene burial based on maximum burial temperatures inferred by AFT data to be >80°C–110°C near Big Fish River and >110°C in Blow Trough and the Barn Mountains (Figure 3a; O'Sullivan & Lane, 1997). To investigate spatial dependencies, we plotted our new AHe results together with previous thermochronology data (Figure 3; Bigot-Buschendorf, 2015; O'Sullivan & Lane, 1997) and on three west–east swath profiles (Figure S9), but could not find any clear correlations.

The AHe date dispersion likely relates to the source rock thermal histories of the individual grains, a concept that we explored using forward modeling (Figure 6). This interpretation is supported by provenance studies that suggest the strata are comprised of recycled grains from the Laurentian craton, the Ellesmerian clastic wedge, and from local strata, with relatively minor contributions from Cordilleran arc sources in younger rocks (e.g., Beranek et al., 2010; Colpron et al., 2018; Hadlari et al., 2015, 2012). These recycled grains with protracted thermal histories have the potential to accumulate significant amounts of radiation damage that affected later helium retentivity. Stratigraphic studies indicate that Lower Cretaceous and older strata of the Richardson Mountains comprise east- and southeast-derived sediment that was deposited on the continental margin of ancestral North America (Figures 7a–7d), whereas Upper Cretaceous–Paleocene rocks comprise west- and southwest-derived sediment deposited in the Cordilleran foreland basin (Figures 7e and 7f; Dixon, 1996a, 2004; Young, 1973). We infer that recycled grains derived from eastern (cratonic and clastic wedge) source rocks cooled relatively slowly and were generally at low temperatures for significant durations before deposition. Conversely, western (Cordilleran) source rocks are more likely to have experienced rapid exhumation through the PRZ before erosion and deposition and therefore have less radiation damage and less dispersion in general. In summary, cratonic grains found in Lower Cretaceous and older strata are more likely to have older apparent cooling ages than the presumably less-damaged Cordilleran grains found in the Upper Cretaceous–Paleocene samples.

The Proterozoic–Cambrian samples yielded well-behaved AHe dates (Figure 4) and thermally reset ZHe dates that suggests burial to >160°C. It is unclear whether Cretaceous–Paleogene burial caused thermal resetting of these samples, or whether these older strata were already buried to temperatures above the AHe PRZ before that time. A Carboniferous–Triassic thermal maximum is well documented across the region and may relate to Ellesmerian foredeep deposition (Lane et al., 2015). AFT data from Devonian rocks in the southern Richardson Mountains (Issler & Lane, 2016; Lane et al., 2015), the Mackenzie Plain
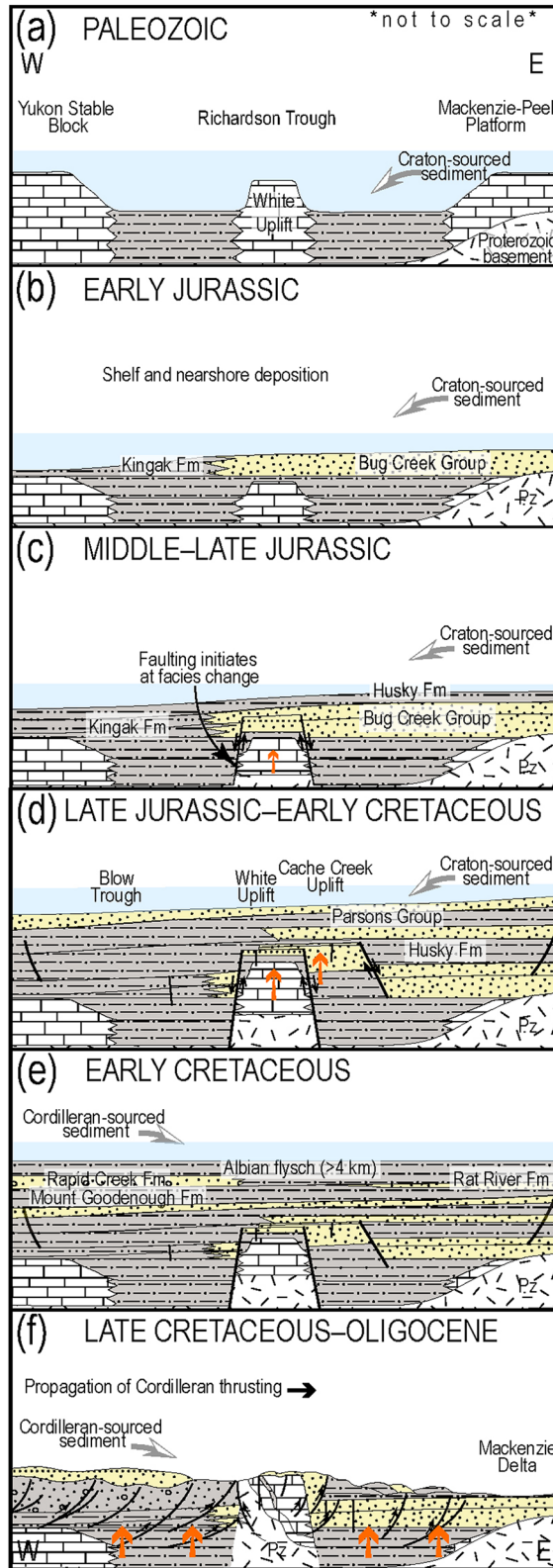
(Issler et al., 2005; Powell et al., 2019), and the plain east of the Mackenzie Delta (Issler et al., 2012) suggest maximum heating to between 90°C–190°C that occurred at least prior to the Middle–Late Triassic. Similar results were obtained from ZHe data of Neoproterozoic strata in the central Mackenzie Mountains (Powell et al., 2016). In the British Mountains, the thermal maximum likely occurred during or before the Early Carboniferous, based on the youngest ZFT age population of partially reset Neoproterozoic rocks (Bigot-Buschendorf et al., 2019). Additionally, thermal maturity data from wells northeast of the Richardson Mountains (Figure 1a) indicate that Permian strata are significantly more mature than overlying Jurassic rocks, reflecting deposition and erosion of ~4 km of strata prior to Jurassic deposition (Issler et al., 2012). Based on these regional trends, we infer that the Proterozoic–Cambrian rocks likely experienced a major burial phase prior to the period of Cretaceous–Paleogene burial.

6.2. Timing and Spatial Pattern of Rock Exhumation

Our new data and previously published data by O'Sullivan and Lane (1997) and Bigot-Buschendorf (2015) suggest that multiple phases of cooling and inferred exhumation due to deformation and erosion affected the northern Richardson Mountains during the Cenozoic (Figure 5). Exhumation initiated in the Paleocene–early Eocene (>65–50 Ma) (Figure 5b; Group 1); followed by a phase of rapid exhumation during late Eocene–early Oligocene time (Figure 5c; Group 2); and exhumation that continued until as late as the early Miocene (Figure 5d; Group 3). The Paleocene–early Eocene cooling and inferred deformation phase corroborates regional structural studies (Lane, 1998; Lane & Dietrich, 1995) and previous findings from AFT data (O'Sullivan & Lane, 1997) that indicate Cordilleran orogenesis affected the northern Richardson Mountains. The AFT data suggest rapid cooling at ~57–53 Ma due to erosion of 2.7–3.8 km of strata (O'Sullivan & Lane, 1997). The late Eocene–early Oligocene deformation phase is supported by some AFT grain dates that are 50–35 Ma, with relatively long (14 μm) confined fission tracks (O'Sullivan & Lane, 1997). Our findings are also supported by AHe results from eight clastic sedimentary rocks in the northwestern part of our study area with ages ranging 42–30 Ma (Figure 3; Bigot-Buschendorf, 2015). This late Eocene–early Oligocene cooling phase was previously not well constrained due to the paucity of data and lack of thermal history modeling in the region. Our modeling results clearly show that deformation and associated cooling occurred regionally during late Eocene–early Oligocene time, after the well-documented initial phase of Paleocene–early Eocene Cordilleran orogenesis. These thermal models show rapid cooling from 70°C–90°C to below 40°C from 40–30 Ma. This cooling suggests at least 0.9–2 km of exhumation, assuming a geothermal gradient of 25°C/km–35°C/km (Dixon, 1996b; O'Sullivan & Lane, 1997). In the northernmost part of our study area, >1.4–3.2 km of rock exhumation occurred during this time to bring sample RM-34 from temperatures of 90°C–110°C to below 40°C (Figure 3). These findings indicate erosion rates of 90–320 m/Myr in the northern Richardson Mountains during late Eocene–Oligocene time. Exhumation that occurred after ~30 Ma is generally not detected by our samples, indicating <1–2 km of exhumation with a maximum erosion rate of 70 m/Myr to bring these rocks to surface today. However, four samples record sensitivity to even later cooling during the late Oligocene–early Miocene (30–15 Ma). These samples may record renewed contraction and reactivation of structures or possibly local continuation of the earlier exhumation.

There is no obvious spatial pattern in the timing of exhumation (Figures 3 and 5 and Figure S9). However, some pre-existing structures such as White Uplift show a clear influence (Figure 3 and Figure S9). The two thrust faults that bound White Uplift (Figure S9d) are assumed to have formed along an important Paleozoic facies change between carbonates of White Uplift and shales of the surrounding Richardson Trough (Figure 7c; Dyke, 1996). The difference in date dispersion and the stratigraphic separation between the samples collected across the thrusts suggest that the Proterozoic–Cambrian rocks (hanging wall) were buried to temperatures above the ZHe PRZ before being rapidly cooled by thrusting and erosion. In comparison, the adjacent Permian–Jurassic rocks (footwall) were within PRZ temperatures before experiencing this final exhumation. We infer from our inverse models (Figure 5) that exhumation of these samples began during

Figure 7. Schematic overview of the geologic history of the study area. (a) Deposition of lower Paleozoic deep-water shales of the Richardson Trough and carbonate platforms, including White Uplift. (b) Deposition of Lower Jurassic nearshore and shelf deposits. (c) Initial faulting at White Uplift at ~170 Ma, causing local erosion of lower Bug Creek Group strata and thinning of the upper Bug Creek Group succession. (d) Late Jurassic–Early Cretaceous block faulting to form Cache Creek Uplift and White Uplift. (e) Deposition of Early Cretaceous Cordilleran foreland strata. (f) Late Cretaceous–Oligocene deformation and associated exhumation of northern Richardson Mountains strata.

the Paleocene–early Eocene to induce cooling through the ZHe PRZ, and was likely renewed during late Eocene–Oligocene. The ZHe data from Proterozoic–Cambrian rocks suggest >4.5–6.4 km of exhumation that occurred during thrust faulting in the Paleocene–early Eocene and late Eocene–Oligocene. Our findings from White Uplift are generally consistent with regional studies that suggest a significant role of inherited structures during Cenozoic deformation (Cook et al., 1987; Hanks, 1993; Lane & Dietrich, 1995).

6.3. Cenozoic Deformation Along the Margin of the Northern Cordillera

The seismically active foreland fold-and-thrust belt along the eastern and northern margin of the Northern Cordillera comprises the northeastern Brooks Range, Richardson Mountains, and Mackenzie Mountains and stretches more than 1,600 km (Figure 1). Previous thermochronology studies along this margin document overall similar timing of deformation during the Late Cretaceous and Cenozoic. Exhumational cooling initiated by ~100 Ma, which is recorded in the Mackenzie Mountains (Enkelmann et al., 2019; Powell et al., 2016), and in the central Brooks Range (Cole et al., 1997; Murphy et al., 1994; O'Sullivan et al., 1997). In the British Mountains, northwest of the Richardson Mountains, deformation initiated slightly later, at ~80 Ma (Bigot-Buschendorf et al., 2019). Migration of the foredeep and propagation of the fold-thrust belt caused an intense phase of deformation at 60–50 Ma, which is indicated in the northern Richardson Mountains by our data and by work by O'Sullivan and Lane (1997). Rapid exhumation at ~60 Ma is also documented across the entire Brooks Range and adjacent foreland basin (e.g., Cole et al., 1997; Craddock et al., 2018; O'Sullivan et al., 1997, 1993; Parris et al., 2003; Potter et al., 2004). Similar results are recorded south of the Richardson Mountains with Paleocene exhumation in the Mackenzie Mountains (Powell et al., 2016) that coincides with maximum burial and heating of Cretaceous strata in the adjacent Mackenzie Plain (Enkelmann et al., 2019; Issler et al., 2005).

Our AHe results indicate another exhumation phase occurred in the northern Richardson Mountains during late Eocene–early Oligocene time (40–30 Ma). These findings are generally consistent with AFT and ZFT data from the northeastern Brooks Range that indicate out-of-sequence deformation during discrete phases at ~45, ~35, and ~25 Ma (Murphy et al., 1994; O'Sullivan, 1996; O'Sullivan & Wallace, 2002; O'Sullivan et al., 1995, 1997; Peapples et al., 1997; Potter et al., 2004). Deformation at ~45 and ~25 Ma is evident across much of the Brooks Range and North Slope (Craddock et al., 2018; Moore et al., 2004; O'Sullivan, 1996; O'Sullivan & Wallace, 2002; O'Sullivan et al., 1997; O'Sullivan, Moore, et al., 1998), whereas deformation at ~35 Ma is recognized only in the northeastern Brooks Range, primarily along the western and northwestern mountain fronts (O'Sullivan, 1992; O'Sullivan & Decker, 1990; O'Sullivan et al., 1993; O'Sullivan, Wallace, et al., 1998). This ~35 Ma deformation phase may correlate with the late Eocene–early Oligocene deformation identified in the Richardson Mountains. However, thermochronology studies between these two disparate regions have not recognized exhumation during this period (e.g., Bigot-Buschendorf, 2015; Bigot-Buschendorf et al., 2019; Lane & Issler, 2011; O'Sullivan et al., 1993).

At the eastern margin of the Mackenzie Mountains and Plain, AHe data from Neoproterozoic–Devonian and Cretaceous rocks evidenced a phase of accelerated cooling during Oligocene–early Miocene time (33–20 Ma) and imply a minimum of 1–3 km of exhumation (Enkelmann et al., 2019). Other authors have interpreted an overall protracted Cenozoic history for strata in the Mackenzie Mountains and Plain based on AFT and AHe data (Powell et al., 2018, 2019). However, these data also indicated a possible Neogene cooling pulse that was not well resolved. A slower cooling history for the northwestern Mackenzie Mountains was interpreted from a single 35 Ma AFT date and overall shortened fission track lengths (Lane & Issler, 2011).

Overall, these results from the Brooks Range, Richardson Mountains, and Mackenzie Mountains indicate that late Eocene to early Miocene (40–20 Ma) cooling due to deformation occurred across the entire northern and eastern margin of the Northern Cordillera. Thrusting and associated rock uplift and erosion caused exhumation of 1–3 km. However, the exact timing of deformation along the margin appears to be asynchronous. Multiple exhumation phases are detected by thermochronology data across the Brooks Range and northern Richardson Mountains, whereas only one phase of deformation is detected in the Mackenzie Mountains during this period. Additionally, there was a 5–10 Myr lag between the main phase of rapid exhumation in the northern Richardson Mountains (40–30 Ma) compared to exhumation in the Mackenzie Mountains (33–20 Ma) and northeastern Brooks Range (~25 Ma).

Seismic and GPS data indicate that the entire margin of the Northern Cordillera is tectonically active and mountain building and deformation is ongoing (Figure 2; Audet & Ma, 2018; Hyndman, Flück, et al., 2005; Leonard et al., 2008). Earthquake focal mechanisms in the Richardson Mountains are predominantly dextral strike-slip (Figure 2; Hyndman, Flück, et al., 2005), which is expected to result in little exhumation compared to dip-slip faulting. However, exhumation elsewhere along the Northern Cordillera margin, characterized by dominantly thrust faulting (Figure 2; Hyndman, Flück, et al., 2005), has also not resulted in exhumation of more than 1–2 km. Thus, the onset of the current deformation phase remains unresolved by thermochronological data and must be recent (post Miocene).

6.4. What Drives Cenozoic Deformation at the Eastern Margin of the Northern Cordillera?

The widespread evidence of late Eocene to early Miocene (40–20 Ma) deformation along the eastern margin of the Northern Cordillera raises questions about possible driving mechanisms. At this time, the Cordilleran compressional deformation is considered to have ended and the western margin of North America was characterized by dextral strike-slip motion and regional transtension (e.g., Dusel-Bacon et al., 2016; Monger & Gibson, 2019). Changes in the direction and velocity of the North American plate motion have been suggested to explain the Oligocene–early Miocene deformation documented in the Mackenzie Mountains (Enkelmann et al., 2019). They propose that the final opening of the North Atlantic may have caused increased rates of NW directed plate motion of the North American craton, which was pushed beneath the weak sedimentary cover strata at the eastern edge of the Northern Cordillera. Similarly, Monger and Gibson (2019) suggested that motion of the North American craton had major influence on the Canadian Cordilleran evolution from ~200 Ma to early Cenozoic. This study reviews the geologic record from mostly the southern and central Canadian Cordillera and found that orogen-normal compression is documented primarily during times of westward craton motion. Dextral and sinistral strike-slip displacement occurred during southwestward and northwestward craton motion, respectively (Monger & Gibson, 2019). Thus, the westward movement of the North American craton, tied to mantle coupling with the thick (>200 km) cratonic lithosphere, is suggested to be the primary driver of the Cordilleran deformation (Monger & Gibson, 2019) and post-Cordilleran deformation along the eastern margin (Enkelmann et al., 2019).

To further explore the kinematic changes of the North American Plate and their possible effect at the eastern margin of the Northern Cordillera, we used GPlates (v2.2; Müller et al., 2018) to track the direction and magnitude of the absolute plate motion since 60 Ma (Figure 8). We used the rotation model of Müller et al. (2019) for our reconstructions and selected three locations along the eastern margin that coincide with availability of thermochronology data at the northeastern Brooks Range, northern Richardson Mountains, and Mackenzie Mountains (Figure 8). Overall, the extracted velocity pattern is similar at these locations at any given time, and show consistently small offsets in magnitude (Figure 9a) and the azimuth (Figure 9b), due to the relative distance from the Euler pole in the North Atlantic. Phases of high plate velocity occurred at 56–48, 40–30, and 10–0 Ma (Figure 9a). Plate velocity was fastest during Paleocene–Eocene time, concurrent with significant Cordilleran deformation across the margin (Figure 9d). The second velocity increase correlates with deformation in the northern Richardson Mountains and parts of the northeastern Brooks Range during late Eocene–Oligocene time. However, the main phase of renewed deformation in the Brooks Range and Mackenzie Mountains started later during the Oligocene when the velocity was starting to decline (Figure 9d). We consider the first-order trend of structures relative to the plate motion vector at each location to evaluate if deformation would be dominated by dip-slip or strike-slip motion. Thermochronology is sensitive to rock exhumation that primarily occurs during dip-slip faulting, when stresses act with a higher angle (>45°) to preexisting structures. Major structures in the northern Richardson Mountains trend NNE and are thus nearly orthogonal to structures in the northeastern Brooks Range (trend E) and Mackenzie Mountains (trend NW) (Figure 8a). We observe a correlation between the obliquity of the plate motion to the main structural trends along the Cordilleran margin and the recorded phases of exhumation. We propose that this difference in structural trend explains the earlier (late Eocene–early Oligocene) exhumation in the Richardson Mountains when plate motion was more normal and resulted in higher dip-slip motion (Figure 9c). The obliquity increases in the Richardson Mountains at 40–35 Ma, coincident with the increase in plate velocity. In comparison, the obliquity decreases to <45° from 40–35 Ma in the northeastern Brooks Range and Mackenzie Mountains, but then increases from 35–20 Ma while the plate velocity is still elevated (Figure 9). This later increase in obliquity coincides with the main phases of recorded exhumation
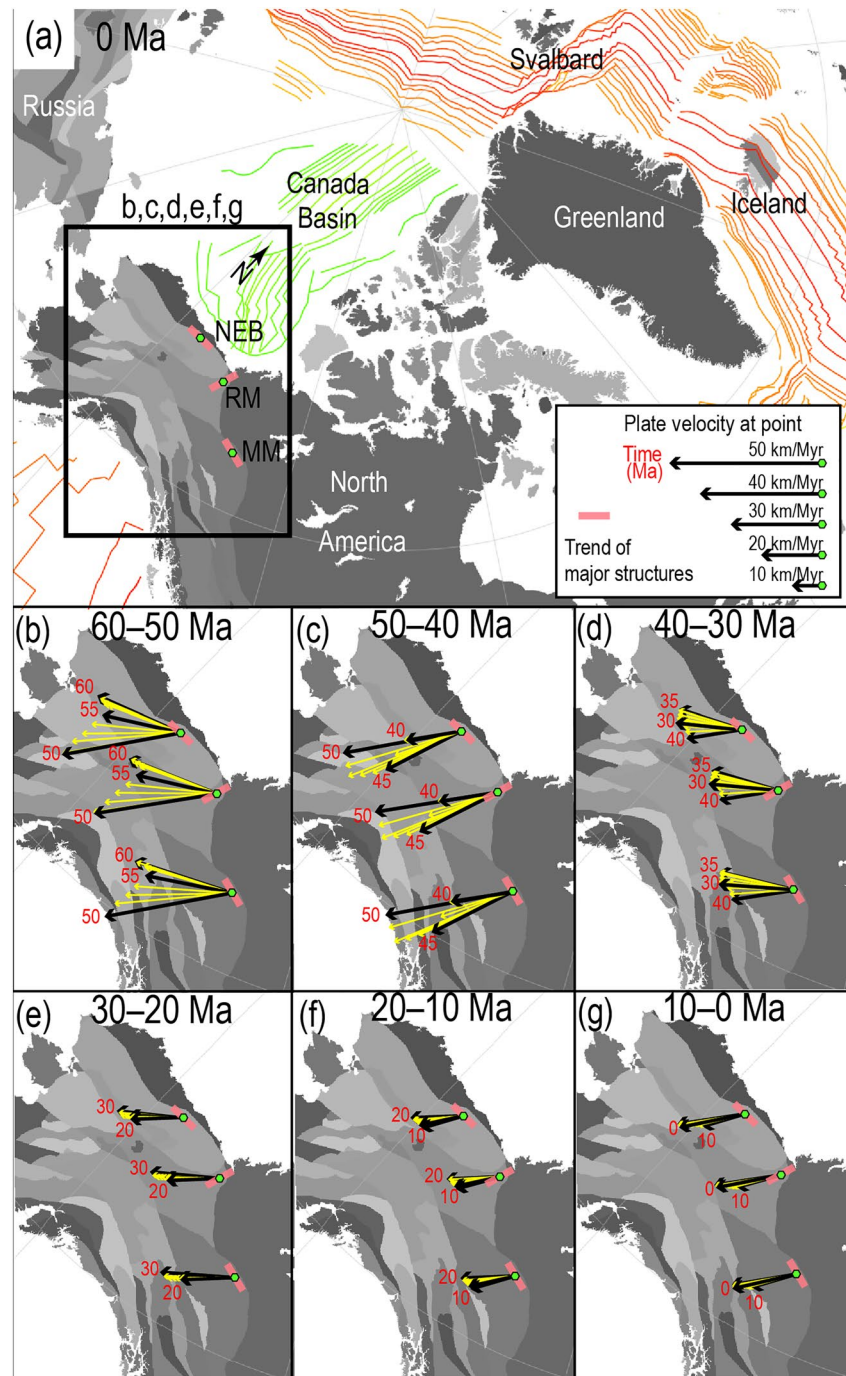
Figure 8. (a) Map of present-day North America showing isochron data related to spreading centers in the Canada Basin and North Atlantic. (b–g) Velocity vectors of the North American Plate from 60 to 0 Ma at locations within the northeastern Brooks Range (NEB), Richardson Mountains (RM), and Mackenzie Mountains (MM), modeled using GPlates (v2.2; Müller et al., 2018). Black arrows represent the velocity vectors at 5 Myr increments. Yellow arrows are velocity vectors at 1 Myr increments.

in these regions. The late Oligocene–early Miocene cooling phase indicated by our thermal history models (Figure 5d) occurred during declining North American plate velocities and moderate obliquity (Figure 9). However, the obliquity to the structures in the Mackenzie Mountains increased and thus resulted in a more distinct record of cooling and suggested initiation of thrusting in the Mackenzie Plain (Enkelmann et al., 2019).
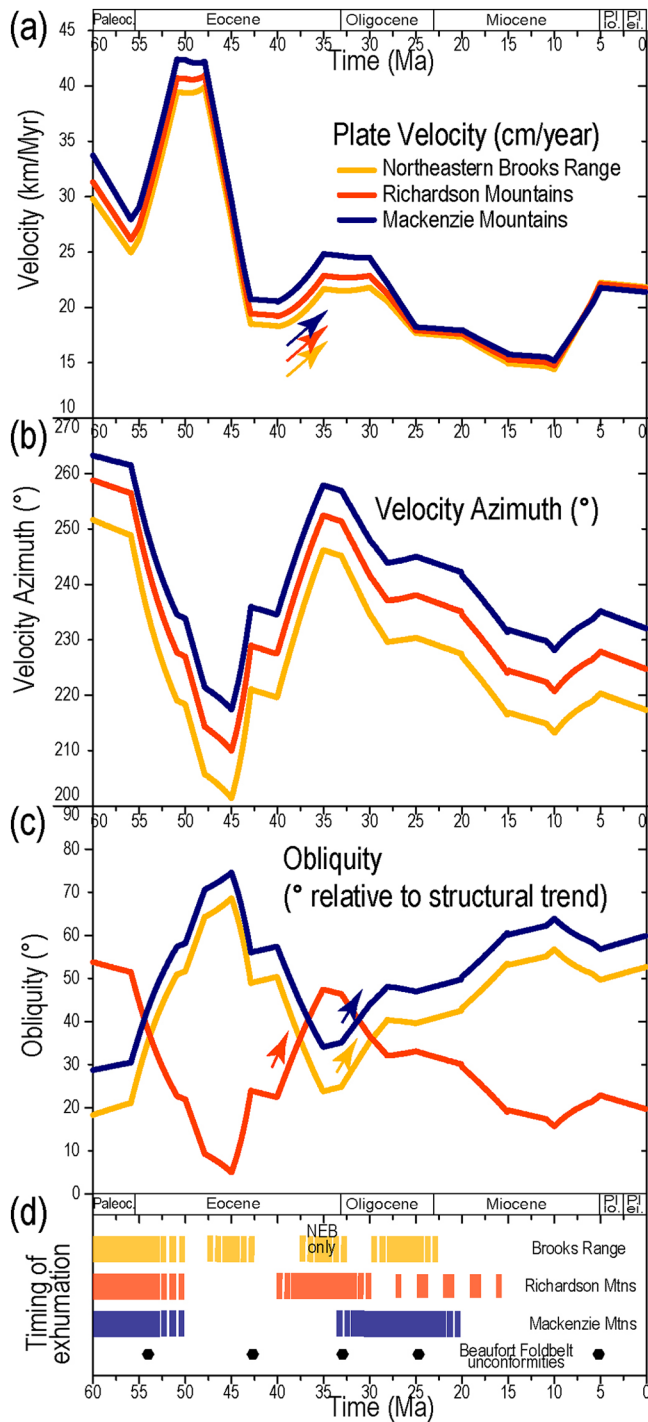
Figure 9. (a–c) Plate kinematics of the eastern margin of the Northern Cordillera since 60 Ma, modeled using GPlates (Müller et al., 2018). Colored arrows refer to kinematic changes referenced in the text. Locations and plate motion vectors are shown in Figure 8. Obliquity refers to the angle between the velocity azimuth and the strike of main structures. (d) Timing of known exhumation phases and offshore unconformities discussed in the text. NEB, northeastern Brooks Range.

We acknowledge that these are simplified structural considerations where the Cordillera is considered the backstop, which is unlikely given its accretion history. More sophisticated models are needed that consider the motion of both, the North American plate and the Cordillera to further investigate the Cenozoic deformation. A possible backstop for craton convergence could be the Resurrection Plate, proposed to have bisected the Kula and Farallon plates until it was fully subducted beneath North America by ~40 Ma (Fuston et al., 2020; Heaussler et al., 2003; Madsen et al., 2006). Tomographic imaging suggests that a remnant of the thermally eroded Resurrection Plate currently underlies the Yukon at a depth of 400–600 km (Fuston et al., 2020). Our GPlates model shows that the last major velocity increase started 10 Ma and may be the onset of the observed deformation pattern today. In summary, we hypothesize that post-Cordilleran exhumation along the eastern margin of the Northern Cordillera was related to the combined effects of westward North American Plate motion and the angle of structural trends relative to the plate motion. Changes in velocity were consistent across the Cordilleran margin, but the obliquity was elevated in the Richardson Mountains approximately 5–10 Myr before the northeastern Brooks Range and Mackenzie Mountains, resulting in a delayed response in exhumation in these latter locations.

7. Conclusions

Analysis of new apatite and zircon (U-Th-Sm)/He data provides insight into the burial and exhumation history of the northern Richardson Mountains (Figure 1). Thermal resetting of the AHe data from Proterozoic–Paleocene rocks suggests burial to >75°C–80°C since deposition. Reset ZHe data from Proterozoic–Cambrian rocks suggests burial to >160°C, whereas unreset ZHe data from Jurassic rocks limits their burial to <160°C. Our analysis of the AHe data yielded three stages of the regional cooling history. Accelerated cooling initiated in the Paleocene–early Eocene (>65–50 Ma), consistent with previous thermochronology data in the region. However, most of our samples underwent rapid cooling during late Eocene–early Oligocene time (40–30 Ma), and some samples cooled during the Oligocene–early Miocene (30–15 Ma). We infer from these cooling histories that the northern Richardson Mountains continued to deform after the Paleocene–early Eocene phase of Cordilleran orogenesis. The cooling decelerated and rocks were close to surface temperatures since the onset of the Miocene. Our data are consistent with studies across the eastern margin of the Northern Cordillera (Figure 1). We propose that this widespread Late Cenozoic exhumation was caused by changes of the North American Plate motion. Measurable exhumation occurred along the eastern margin of the Northern Cordillera during periods of increased plate velocity, particularly when plate motion was at higher angle to preexisting structures.

Data Availability Statement

All new data presented in this manuscript are publicly available at https://www.geochron.org/results.php?pkey=32074.

References

Armstrong, P. A. (2005). Thermochronometers in sedimentary basins. *Reviews in Mineralogy and Geochemistry*, *58*, 499–525.

Audet, P., & Ma, S. (2018). Deep crustal earthquakes in the Beaufort Sea, Western Canadian Arctic, from teleseismic depth phase analysis. *Seismological Research Letters*, *89*(4), 1379–1384. https://doi.org/10.1785/0220180047

Beranek, L. P., Mortensen, J. K., Lane, L. S., Allen, T. L., Fraser, T. A., Hadlari, T., & Zantvoort, W. G. (2010). Detrital zircon geochronology of the western Ellesmerian clastic wedge, northwestern Canada: Insights on Arctic tectonics and the evolution of the northern Cordilleran miogeocline. *GSA Bulletin*, *122*(11/12), 1899–1911. https://doi.org/10.1130/B30120.1

Bigot-Buschendorf, M. (2015). *Evolution thermo-cinématique et géodynamique du Brooks Range et du North Slope (Alaska-Canada)* (Doctoral dissertation, p. 335). Paris VI, Français: Sciences de la Terre. Université Pierre et Marie Curie.

Bigot-Buschendorf, M., Mouthereau, F., Labrousse, L., Fillon, C., Stübner, K., & Bernet, M. (2019). Unravelling the thermal evolution of the Neruokpuk Formation in the British Mountains, North Yukon, Canada: Tectonic and orogenic implications. In K. Piepjohn, J. V. Strauss, L. Reinhardt, & W. C. McClelland (Eds.), *Circum-Arctic structural events: Tectonic evolution of the Arctic margins and trans-Arctic links with adjacent orogens* (pp. 619–635): Geological Society of America Special Paper 541. https://doi.org/10.1130/2018.2541(26)

Blythe, A. E., Bird, J. M., & Omar, G. I. (1996). Deformational history of the central Brooks Range, Alaska: Results from fission-track and $^{40}Ar/^{39}Ar$ analyses. *Tectonics*, *15*(2), 440–455.

Blythe, A. E., Murphy, J., & O'Sullivan, P. B. (1997). Tertiary cooling and deformation in the south-Central Brooks Range: Evidence from zircon and apatite fission-track analyses. *The Journal of Geology*, *105*(5), 583–600.

Cole, F., Bird, K. J., Toro, J., Roure, F., O'Sullivan, P. B., Pawlewicz, M., & Howell, D. G. (1997). An integrated model for the tectonic development of the frontal Brooks Range and Colville Basin 250 km west of the Trans-Alaska crustal transect. *Journal of Geophysical Research*, *102*(B9), 20685–20708.

Colpron, M., McLelland, W. C., & Strauss, J. V. (2018). Detrital zircon U-Pb geochronological and Hf isotopic constraints on the geological evolution of North Yukon. In K. Piepjohn, J. V. Strauss, L. Reinhardt, & W. C. McClelland (Eds.), *Circum-Arctic structural events: Tectonic evolution of the Arctic margins and Trans-Arctic links with adjacent orogens* (pp. 397–437): Geological Society of America Special Paper 541. https://doi.org/10.1130/2018.2541(19)

Cook, F. A., Coffin, K. C., Lane, L. S., Dixon, J., & Dietrich, J. R. (1987). Structure of the southeast margin of the Beaufort-Mackenzie Basin, Arctic Canada, from crustal seismic reflection data. *Geology*, *15*, 931–935.

Craddock, W. H., Moore, T. E., O'Sullivan, P. B., Potter, C. J., & Houseknecht, D. W. (2018). Late Cretaceous-Cenozoic exhumation of the western Brooks Range, Alaska, revealed from apatite and zircon fission track data. *Tectonics*, *37*, 4714–4751. https://doi.org/10.1029/2018TC005282

Dixon, J. (1992). A review of Cretaceous and Tertiary stratigraphy in the northern Yukon and adjacent Northwest Territories. *Geological Survey of Canada Paper*, *92*(9), 1–79.

Dixon, J. (1993). Regional unconformities in the Cretaceous of northwest Canada. *Cretaceous Research*, *14*, 17–38.

Dixon, J. (1996a). Cretaceous and tertiary. In D. K. Norris (Ed.), *The geology, mineral and hydrocarbon potential of northern Yukon Territory and northwestern District of Mackenzie* (Vol. 422, pp. 301–317). Geological Survey of Canada, Bulletin.

Dixon, J. (1996b). Stratigraphy and structure. In J. Dixon (Ed.), *Geological atlas of the Beaufort-Mackenzie area* (Miscellaneous Report 59, pp. 39–88). Geological Survey of Canada.

Dixon, J. (2004). Jurassic–Lower Cretaceous (Oxfordian to lower Aptian) strata, Yukon Territory-Northwest Territories. In *Geological Atlas of the Northern Canadian Mainland Sedimentary Basin* (Open File 4633). Geological Survey of Canada.

Dixon, J., Dietrich, J. R., & McNeil, D. H. (1992). Upper Cretaceous sequence stratigraphy of the Beaufort-Mackenzie and Banks Island areas, northwest Canada (Vol. 407, p. 90). Geological Survey of Canada, Bulletin.

Dusel-Bacon, C., Bacon, C. R., O'Sullivan, P. B., & Day, W. C. (2016). Apatite fission-track evidence for regional exhumation in the subtropical Eocene, block faulting, and localized fluid flow in east-central Alaska. *Canadian Journal of Earth Sciences*, *53*, 260–280. https://doi.org/10.1139/cjes-2015-0138

Dyke, L. D. (1996). White, Barn and Campbell uplifts. In D. K. Norris (Ed.), *The geology, mineral and hydrocarbon potential of northern Yukon Territory and northwestern District of Mackenzie* (Vol. 422, pp. 333–358). Geological Survey of Canada, Bulletin.

Earthquakes Canada. (2019). *Geological Survey of Canada, Earthquake Search*. Retrieved from http://earthquakescanada.nrcan.gc.ca

Enkelmann, E., Finzel, E., & Arkle, J. (2019). Deformation at the eastern margin of the Northern Canadian Cordillera: Potentially related to opening of the North Atlantic. *Terra Nova*, *31*, 151–158. https://doi.org/10.1111/ter.12374

Evans, N. J., Byrne, J. P., Keegan, J. T., & Dotter, L. E. (2005). Determination of uranium and thorium in zircon, apatite, and fluorite: Application to laser (U-Th)/He thermochronology. *Journal of Analytical Chemistry*, *60*(12), 1159–1165.

Farley, K. A. (2000). Helium diffusion from apatite: General behavior as illustrated by Durango fluorapatite. *Journal of Geophysical Research*, *105*, 2903–2914.

Farley, K. A., Wolf, R. W., & Silver, L. T. (1996). The effects of long alpha-stopping distances on (U-Th)/He ages. *Geochimica et Cosmochimica Acta*, *60*, 4223–4229.

Farley, K., Shuster, D., & Ketcham, R. (2011). U and Th zonation in apatite observed by laser ablation ICPMS, and implications for the (U–Th)/He system. *Geochimica et Cosmochimica Acta*, *75*(16), 4515–4530. https://doi.org/10.1016/j.gca.2011.05.020

Flowers, R., Ketcham, R. A., Shuster, D. L., & Farley, K. A. (2009). Apatite (U–Th)/He thermochronometry using a radiation damage accumulation and annealing model. *Geochimica et Cosmochimica Acta*, *73*, 2347–2365. https://doi.org/10.1016/j.gca.2009.01.015

Fox, M., Dai, J.-G., & Carter, A. (2019). Badly behaved detrital (U-Th)/He ages: Problems with He diffusion models or geological models? *Geochemistry, Geophysics, Geosystems*, *20*, 2418–2432. https://doi.org/10.1029/2018GC008102

Fuston, S. & Wu, J. (2020). Raising the Resurrection plate from an unfolded-slab plate tectonic reconstruction of northwestern North America since early Cenozoic time. *GSA Bulletin*. https://doi.org/10.1130/B35677.1

Gautheron, C., Tassan-Got, L., Ketcham, R. A., & Dobson, K. J. (2012). Accounting for long alpha-particle stopping distances in (U–Th–Sm)/He geochronology: 3D modeling of diffusion, zoning, implantation, and abrasion. *Geochimica et Cosmochimica Acta*, *96*, 44–56. https://doi.org/10.1016/j.gca.2012.08.016

Grantz, A., Hart, P., & Childers, V. (2011). Geology and tectonic development of the Amerasia and Canada Basins, Arctic Ocean. In A. M. Spencer, A. F. Embry, D. L. Gautier, A. V. Stoupakova, & K. Sørensen (Eds.), *Arctic Petroleum Geology, Geological Society (London) Memoirs* (Vol. 35, pp. 771–799). https://doi.org/10.1144/M35.50

Guenthner, W. R., Reiners, P. W., DeCelles, P. G., & Kendall, J. (2015). Sevier belt exhumation in central Utah constrained from complex zircon (U-Th)/He data sets: Radiation damage and He inheritance effects on partially reset detrital zircons. *GSA Bulletin*, *127*(3), 323–348. https://doi.org/10.1130/B31032.1

Guenthner, W. R., Reiners, P. W., Ketcham, R. A., Nasdala, L., & Giester, G. (2013). Helium diffusion in natural zircon: Radiation damage, anisotropy, and the interpretation of zircon (U-Th)/He thermochronology. *American Journal of Science*, *313*, 145–198. https://doi.org/10.2475/03.2013.01

Hadlari, T., Davis, W. J., Dewing, K., Heaman, L. M., Lemieux, Y., Ootes, L., et al. (2012). Two detrital zircon signatures for the Cambrian passive margin of northern Laurentia highlighted by new U-Pb results from northern Canada. *GSA Bulletin*, *124*(7/8), 1155–1168. https://doi.org/10.1130/B30530.1

Hadlari, T., Swindles, G. T., Galloway, J. M., Bell, K. M., Sulphur, K. C., Heaman, L. M., et al. (2015), 1.8 billion years of detrital zircon recycling calibrates a refractory part of earth's sedimentary cycle. *PLoS One*, *10*(12), 10. https://doi.org/10.1371/journal.pone.0144727

Haeussler, P. J., Bradley, D. C., Wells, R. E., & Miller, M. L. (2003). Life and death of the Resurrection plate: Evidence for its existence and subduction in the northeastern Pacific in Paleocene–Eocene time. *GSA Bulletin*, *115*(7), 867–880.

Hanks, C. L. (1993). The Cenozoic structural evolution of a fold-and-thrust belt, northeastern Brooks Range, Alaska. *GSA Bulletin*, *105*, 287–305.

Harrison, T. M., & Zeitler, P. K. (2005). Fundamentals of noble gas thermochronometry. *Reviews in Mineralogy and Geochemistry*, *58*, 123–149. https://doi.org/10.2138/rmg.2005.58.5

Helwig, J., Kumar, N., Emmet, P., & Dinkelman, M. G. (2011). Regional seismic interpretation of crustal framework, Canadian Arctic passive margin, Beaufort Sea, with comments on petroleum potential. In A. M. Spencer, A. F. Embry, D. L. Gautier, A. V. Stoupakova, & K. Sørensen (Eds.), *Arctic Petroleum Geology, Geological Society (London) Memoirs* (Vol. 35, pp. 527–543). https://doi.org/10.1144/M35.35

Hyndman, R. D., Cassidy, J. F., Adams, J., Rogers, G. C., & Mazzotti, S. (2005). Earthquakes and seismic hazard in the Yukon-Beaufort-Mackenzie. *CSEG Recorder*, 33–45.

Hyndman, R. D., Flück, P., Mazzotti, S., Lewis, T. J., Ristau, J., & Leonard, L. (2005). Current tectonics of the northern Canadian Cordillera. *Canadian Journal of Earth Sciences*, *42*, 1117–1136. https://doi.org/10.1139/E05-023

Issler, D., Reyes, J., Zhuoheng, C., Kezhen, H., Negulic, E., Grist, A., et al. (2012). Thermal history analysis of the Beaufort-Mackenzie Basin, Arctic Canada. In N. C. Rosen, P. Weimer, S. M. Coutes dos Anjos, S. Henrickson, E. Marques, M. Mayall, et al. (Eds.), *New understanding of the petroleum systems of continental margins of the world* (pp. 609–640). 32nd Annual GCSSEPM Foundation Bob F. Perkins Research Conference, 2012.

Issler, D. R., Grist, A. M., & Stasiuk, L. D. (2005). Post-Early Devonian thermal constraints on hydrocarbon source rock maturation in the Keele Tectonic Zone, Tulita area, NWT, Canada, from multi-kinetic apatite fission track thermochronology, vitrinite reflectance and shale compaction. *Bulletin of Canadian Petroleum Geology*, *53*(4), 405.–431.

Issler, D. R., & Lane, L. S. (2016). *Report of activities for the GEM-2 multi-kinetic apatite fission track (MK-AFT) modeling and method development* (Open File 8147, p. 12): Geological Survey of Canada.

Jeletzky, J. A. (1963). Pre-Cretaceous Richardson Mountains trough—Its place in the tectonic framework of Arctic Canada and its bearing on some geosynclinal concepts. *Royal Society of Canada, Transactions*, *56*(3), 55–84.

Ketcham, R. A. (2005). Forward and inverse modeling of low-temperature thermochronometry data. *Reviews in Mineralogy and Geochemistry*, *58*, 275–314.

Lane, L. S. (1996). Geometry and tectonics of early Tertiary triangle zones, northeast Eagle Plain, Yukon Territories. *Bulletin of Canadian Petroleum Geology*, *44*, 337–348.

Lane, L. S. (1998). Latest Cretaceous–Tertiary tectonic evolution of Northern Yukon and adjacent Arctic Alaska. *AAPG Bulletin*, *82*(7), 1353–1371.

Lane, L. S. (2007). Devonian–Carboniferous paleogeography and orogenesis, northern Yukon and adjacent Arctic Alaska. *Canadian Journal of Earth Sciences*, *44*, 679–694. https://doi.org/10.1139/E06-131

Lane, L. S., & Dietrich, J. R. (1995). Tertiary structural evolution of the Beaufort Sea-Mackenzie Delta region, Arctic Canada. *Bulletin of Canadian Petroleum Geology*, *43*, 293–314.

Lane, L. S., & Issler, D. R. (2011). *Overview of the Tertiary cooling-uplift history of northernmost Yukon adjacent to the Beaufort Basin, based on apatite fission track studies [Abstract]*. 2011 CSPG-CSEG-CWLS Annual Convention, Calgary, CA. Abstract number 196s0128.

Lane, L. S., Issler, D. R., & O'Sullivan, P. B. (2015). *Late Paleozoic thermochronology of Northern Yukon: Implications for Phanerozoic basin evolution in northern Canada [Abstract]*. GeoConvention 2015: Geoscience New Horizons, CSPG-CSEG-CWLS Annual Convention. Calgary, CA: Telus Convention Centre.

Lane, L. S., & Mortensen, J. K. (2019). U–Pb geochronology, Nd–Sm geochemistry, structural setting, and tectonic significance of Late Devonian and Paleogene intrusions in northern Yukon and northeastern Alaska. *Canadian Journal of Earth Sciences*, *56*, 585–606. https://doi.org/10.1139/cjes-2018-0131

Leonard, L. J., Mazzotti, S., & Hyndman, R. D. (2008). Deformation rates from earthquakes in the northern Cordillera of Canada and eastern Alaska. *Journal of Geophysical Research*, *113*, B08406. https://doi.org/10.1029/2007JB005456

Müller, R. D., Cannon, J., Qin, X., Watson, R. J., Gurnis, M., Williams, S., et al. (2018). GPlates: Building a virtual Earth through deep time. *Geochemistry, Geophysics, Geosystems*, *19*, 2243–2261. https://doi.org/10.1029/2018GC007584

Müller, R. D., Zahirovic, S., Williams, S. E., Cannon, J., Seton, M., Bower, D. J., et al. (2019). A global plate model including lithospheric deformation along major rifts and orogens since the Triassic. *Tectonics*, *38*, 1884–1907.

Madsen, J. K., Thorkelson, D. J., Friedman, R. M., & Marshall, D. D. (2006). Cenozoic to Recent plate configurations in the Pacific Basin: Ridge subduction and slab window magmatism in western North America. *Geosphere*, *2*(1), 11–34. https://doi.org/10.1130/GES00020.1

Mazzotti, S., & Hyndman, R. D. (2002). Yakutat collision and strain transfer across the northern Canadian Cordillera. *Geology*, *30*, 495–498.

Monger, J. W. H., & Gibson, D. H. (2019). Mesozoic-Cenozoic deformation in the Canadian Cordillera: The record of a "Continental Bulldozer"? *Tectonophysics*, *757*, 153–169. https://doi.org/10.1016/j.tecto.2018.12.023

Moore, T. E., Potter, C. J., O'Sullivan, P. B., Shelton, K. L., & Underwood, M. B. (2004). Two stages of deformation and fluid migration in the west central Brooks Range fold and thrust belt, northern Alaska. In F. Roure, J. W. Granath, & R. Swenson (Eds.), *Deformation, fluid flow, and reservoir appraisal in foreland fold and thrust belts* (pp. 157–186). Tulsa, Oklahoma: American Association of Petroleum Geologists Hedberg Series.

Morrow, D. W. (1999). Lower Paleozoic stratigraphy of northern Yukon Territory and northwestern District of Mackenzie (Vol. 538): Geological Survey of Canada, Bulletin.

Murphy, J. M., O'Sullivan, P. B., & Gleadow, A. J. W. (1994). Apatite fission track evidence of episodic Early Cretaceous to Late Tertiary cooling and uplift events, Central Brooks Range, Alaska. In D. K. Thurston, & K. Fujita (Eds.), *Proceedings First Int. Conference on Arctic Margins, 1992* (pp. 257–262). Anchorage, AK.

Norris, D. K. (1996). Geological setting. In D. K. Norris (Ed.), *The geology, mineral and hydrocarbon potential of northern Yukon Territory and northwestern District of Mackenzie* (Vol. 422, pp. 21–64): Geological Survey of Canada, Bulletin.

O'Sullivan, P. B. (1992). Timing of Tertiary episodes of cooling in response to uplift and erosion, northeastern Brooks Range, Alaska. In D. Thurston, & K. Fujita (Eds.), *Proceedings Int. Conf. on Arctic Margins, U.S. Minerals Management Service Outer Continental Shelf Study 94-0040* (pp. 269–274).

O'Sullivan, P. B. (1996). Late Mesozoic and Cenozoic thermal-tectonic evolution of the North Slope foreland basin, Alaska. In M. J. Johnsson, & D. G. Howell (Eds.), *Thermal evolution of sedimentary basins in Alaska* (Vol. 2142, pp. 45–79). U.S. Geological Survey Bulletin.

O'Sullivan, P. B., & Decker, J. (1990). Apatite fission track evidence for Paleocene and Oligocene uplift events in the Northeastern Brooks Range, Alaska. *International Journal of Radiation Applications and Instrumentation, Part D: Nuclear Tracks and Radiation Measurements*, *17*(3), 367–371.

O'Sullivan, P. B., Green, P. F., Bergman, S. C., Decker, J., Duddy, I. R., Gleadow, A. J. W., & Turner, D. L. (1993). Multiple phases of Tertiary uplift and erosion in the Arctic National Wildlife Refuge, Alaska, revealed by apatite fission track analysis. *American Association of Petroleum Geologists Bulletin*, *77*, 359–385.

O'Sullivan, P. B., Hanks, C. L., Wallace, W. K., & Green, P. F. (1995). Multiple episodes of Cenozoic denudation in the north-eastern Brooks Range: Fission-track data from the Okpilak batholith, Alaska. *Canadian Journal of Earth Sciences*, *32*, 1106–1118.

O'Sullivan, P. B., & Lane, L. S. (1997). Early Tertiary thermotectonic history of northern Yukon and adjacent Northwest Territories, Arctic Canada. *Canadian Journal of Earth Sciences*, *34*, 1366–1378.

O'Sullivan, P. B., Moore, T. E., & Murphy, J. M. (1998a). Tertiary uplift of the Mt. Doonerak antiform, central Brooks Range, Alaska: Apatite fission track evidence from the Trans-Alaska crustal transect. In S. Oldow, & H. G. Ave Lallemant (Eds.), *Architecture of a fold and thrust belt: Central Brooks Range, Arctic Alaska* (Vol. 324, pp. 179–194): Geological Society of America Special Paper.

O'Sullivan, P. B., Murphy, J. M., & Blythe, A. E. (1997). Late Mesozoic and Cenozoic thermotectonic evolution of the central Brooks Range and adjacent North Slope foreland basin, Alaska: Including fission track results from the Trans-Alaska Crustal Transect (TACT). *Journal of Geophysical Research*, *102*(B9), 20821–20845.

O'Sullivan, P. B., & Wallace, W. K. (2002). Out-of-sequence, basement-involved structures in the Sadlerochit Mountains region of the Arctic National Wildlife Refuge, Alaska: Evidence and implications from fission-track thermochronology. *GSA Bulletin*, *114*(11), 1356–1378.

O'Sullivan, P. B., Wallace, W. K., & Murphy, J. M. (1998b). Fission-track evidence for apparent out-of-sequence Cenozoic deformation along the Philip Smith Mountain front, Northeastern Brooks Range, Alaska. *Earth and Planetary Science Letters*, *164*, 435–449.

Parris, T. M., Burruss, R. C., & O'Sullivan, P. B. (2003). Deformation and the timing of gas generation and migration in the eastern Brooks Range foothills, Arctic National Wildlife Refuge, Alaska. *AAPG Bulletin*, *87*(11), 1823–1846.

Peapples, P. R., Wallace, W. K., Hanks, C. L., O'Sullivan, P. B., & Layer, P. W. (1997). Style, controls, and timing of fold-and-thrust deformation of the Jago stock, northeastern Brooks Range, Alaska. *Canadian Journal of Earth Sciences*, *34*(7), 992–1007.

Pease, V., Drachev, S., Stephenson, R., & Zhang, X. (2014). Arctic lithosphere—A review. *Tectonophysics*, *628*, 1–25. https://doi.org/10.1016/j.tecto.2014.05.033

Potter, C. J., Grow, J. A., Perry, W. J., Moore, T. E., O'Sullivan, P. B., Phillips, J. D., & Saltus, R. W. (2004). Tertiary thrust systems and fluid flow beneath the Beaufort coastal plain (1002 Area), Arctic National Wildlife Refuge, Alaska, U.S.A. In R. Swennen, F. Roure, & J. W. Granath (Eds.), *Deformation, fluid flow, and reservoir appraisal in foreland fold and thrust belts* (Vol. 1, pp. 187–214). AAPG Hedberg Series. https://doi.org/10.1306/1025691H13117

Poulton, T., Leskiw, K., & Audretsch, A. (1982). Stratigraphy and microfossils of the Jurassic Bug Creek Group of northern Richardson Mountains, northern Yukon and adjacent Northwest Territories. *Geological Survey of Canada Bulletin*, *325*, 1–137.

Poulton, T. P. (1996). Jurassic. In D. K. Norris (Ed.), *The geology, mineral and hydrocarbon potential of northern Yukon Territory and northwestern District of Mackenzie* (Vol. 422, pp. 267–299): Geological Survey of Canada, Bulletin.

Powell, J. W., Issler, D. R., Schneider, D. A., Fallas, K. M., & Stockli, D. F. (2019). Thermal history of the Mackenzie Plain, Northwest Territories, Canada: Insights from low-temperature thermochronology of the Devonian Imperial Formation. *GSA Bulletin*, *132*(3/4), 767–783. https://doi.org/10.1130/B35089.1

Powell, J. W., Schneider, D. A., & Issler, D. R. (2018). Application of multi-kinetic apatite fission track and (U-Th)/He thermochronology to source rock thermal history: A case study from the Mackenzie Plain, NWT, Canada. *Basin Research*, *30*, 497–512. https://doi.org/10.1111/bre.12233

Powell, J. W., Schneider, D. A., Stockli, D. F., & Fallas, K. M. (2016). Zircon (U-Th)/He thermochronology of Neoproterozoic strata from the Mackenzie Mountains, Canada: Implications for the Phanerozoic exhumation and deformation history of the northern Canadian Cordillera. *Tectonics*, *35*, 663–689. https://doi.org/10.1002/2015TC003989

Rohr, K. M., Lane, L. S., & MacLean, B. C. (2011). Subsurface compressional structures and facies transitions imaged by seismic reflection data, eastern margin of Richardson Trough, Peel Plateau, Yukon. *Bulletin of Canadian Petroleum Geology*, *59*(2), 131–146.

Shuster, D. L., & Farley, K. A. (2009). The influence of artificial radiation damage and thermal annealing on helium diffusion kinetics in apatite. *Geochimica et Cosmochimica Acta*, *73*, 183–196. https://doi.org/10.1016/j.gca.2008.10.013

Shuster, D. L., Flowers, R. M., & Farley, K. A. (2006). The influence of natural radiation damage on helium diffusion kinetics in apatite. *Earth and Planetary Science Letters*, *249*, 148–161. https://doi.org/10.1016/j.epsl.2006.07.028

Wolf, R. A., Farley, K. A., & Kass, D. (1998). Modeling of the temperature sensitivity of the apatite (U–Th)/He thermochronometer. *Chemical Geology*, *148-1*, 105–114.

Wolf, R. A., Farley, K. A., & Silver, L. T. (1996). Helium diffusion and low temperature thermochronometry of apatite. *Geochimica et Cosmochimica Acta*, *60*, 4231–4240.

Young, F. G. (1973). Mesozoic epicontinental, flyschoid and molassoid depositional phases of Yukon's north slope. In J. D. Aitken, & D. J. Glass (Eds.), *Geology of the Canadian Arctic* (pp. 181–204). Geological Association of Canada–Canadian Society of Petroleum Geologists.

Young, F. G. (1977). The mid-Cretaceous flysch and phosphatic ironstone sequence, northern Richardson Mountains, Yukon territory. In R. G. Blackadar, P. J. Griffin, H. Dumych, & E. J. W. Irish, (Eds.), *Report of activities, part C*, Geological Survey of Canada, Paper 77-1C (p. 115). Natural Resources Canada. https://doi.org/10.4095/119798